AIAA 81-0300R

Simulation of Atmospheric Turbulent Gusts and Gust Gradients

Frank B. Tatom* and Stephen R. Smith†
Engineering Analysis, Inc., Huntsville, Ala.
and
George H. Fichtl‡ and C. Warren Campbell§
NASA Marshall Space Flight Center, Marshall Space Flight Center, Ala.

An improved three-dimensional, nonrecursive model for atmospheric turbulence has been developed that provides for simulation of both instantaneous gusts and gust gradients along the flight path of the Space Shuttle. The one-dimensional gust and gust gradient spectral models, which form the basis for the simulation scheme, are developed from three-dimensional, von Kármán spectra, integrated over finite limits based on the characteristic dimensions (length, width, and thickness) of the flight vehicle. By means of the simulation process, non-dimensional time series for both gusts and gust gradients have been generated and stored on a series of magnetic tapes for four altitude bands ranging from 0 to 10,000 m. These Shuttle Simulation Turbulence Tapes (SSTT) have been validated by means of spectral and statistical analyses with very satisfactory results. The dimensionless form of the time series, coupled with the use of a von Kármán spectral model (as opposed to a Dryden model), distinguish the SSTT from earlier turbulence simulation concepts.

Nomenclature¶

a = von Kármán constant = 1.339
$\partial u_i/\partial x_j$ = gradient of ith gust component with respect to jth coordinate
$h(j)$ = discrete form of double-sided impulse response function = $h(jT)$
$h(t)$ = double-sided impulse response function
$H(\Omega_1)$ = double-sided Fourier transform of $h(t)$
$I(j)$ = discrete form of white noise = $I(jT)$
$I(t)$ = white noise
k = magnitude of wave number, rad m^{-1}
k_i = ith component of wave number, rad m^{-1}
ℓ_i = characteristic dimension of vehicle, m
L_i = integral scale of turbulence associated with the $\Phi_{ii}(\Omega_1)$ spectrum, m
L_{in} = integral scale of turbulence L_i corresponding to altitude z_n, m
M = expected number of exceedances per unit time, h^{-1}
p_i = exponent for low-altitude variation of σ_i
q_i = exponent for low-altitude variation of L_i
R_{ij} = cross-correlation coefficient for u_i and u_j
t'_e = exposure time, h
t'_i = time for the ith component of turbulence, s
t'_{iN} = time corresponding to N time increments for the ith component of turbulence, s
T = time interval = $\pi/\Omega_{1\max}$
$\bar{u}$ = mean wind velocity, m s^{-1}
u_i = ith component of turbulence gust
u^*_0 = surface friction velocity, m s^{-1}
V = vehicle speed, m s^{-1}
V_n = vehicle speed corresponding to altitude z_n, m s^{-1}
x_j = spatial coordinate
$Y(t)$ = output of digital filter
$Y(m)$ = discrete form of output of digital filter = $Y(mT)$
z = altitude, m
z_n = altitude corresponding to nth step in trajectory, m
$\Delta t'_i$ = time step for the ith component of turbulence, s
$\Delta t'_{in}$ = time increment corresponding to nth step in trajectory for the ith component of turbulence, s
ξ = gust velocity threshold value, m s^{-1}
σ_i = ith component of standard deviation, m s^{-1}
$\phi_{ii}(\Omega_1, \Omega_2, \Omega_3)$ = double-sided, three-dimensional spectrum for u_i gust
$\phi_{ii/jj}(\Omega_1, \Omega_2, \Omega_3)$ = double-sided, three-dimensional spectrum for $\partial u_i/\partial x_j$ gust gradient
$\Phi_{DI}(\Omega_1)$ = double-sided, one-dimensional spectrum of $I(t)$
$\Phi_{DY}(\Omega_1)$ = double-sided, one-dimensional spectrum of $Y(t)$
$\Phi_{ii}(\Omega_1)$ = single-sided, one-dimensional spectrum for u_i gust
$\Phi_{ii/jj}(\Omega_1)$ = single-sided, one-dimensional spectrum for $\partial u_i/\partial x_j$ gust gradient
$\Phi_Y(\Omega_1)$ = single-sided, one-dimensional spectrum of $Y(t)$
ω_i = ith component of frequency, rad s^{-1}
Ω = magnitude of frequency = aLk
Ω_1 = longitudinal component of frequency = aL_1k_1 or $aL_1\omega_1/V$
Ω_i = ith component of frequency = aL_ik_i
$\Omega_{i\max}$ = finite upper limit for Ω_i
Ω_{NG} = Nyquist generation frequency
Ω_{NS} = Nyquist sampling frequency

Superscripts

$()^*$ = complex conjugate
$()'$ = dimensional

Subscripts

1 = longitudinal
2 = lateral
3 = vertical

Presented as Paper 81-0300 at the AIAA 19th Aerospace Sciences Meeting, St. Louis, Mo., Jan. 12-15, 1981; submitted March 4, 1981; revision received July 27, 1981.

*President.
†Member of the Technical Staff.
‡Chief, Fluid Dynamics Branch, Space Sciences Laboratory. Associate Fellow AIAA.
§Aerospace Engineer, Fluid Dynamics Branch, Space Sciences Laboratory.

¶All terms are dimensionless unless otherwise noted.

I. Introduction

THE effects of atmospheric turbulence in both horizontal and near-horizontal flight during the return of the Space Shuttle are important for determining design, control, and "pilot-in-the-loop" effects. All existing simulated turbulence models appear to be dimensional in form and most are based on Dryden spectra. Perhaps the only recent technique that employs von Kármán spectra is the "four-point model" developed by Etkin,[1] based on earlier work by Skelton[2] and Holley and Bryson.[3] The four-point model, which is dimensional, side-steps the problem of simulating gust gradients by simulating turbulence time histories at selected points on the vehicle (center-of-gravity, tail, and each wing), and then by finite-differencing, obtains estimates of gust gradients. This technique avoids the issue of specifying wave-number cutoffs to obtain gust gradient spectra, but replaces this consideration with an estimation of length scales over which the finite-differencing must be performed to obtain the gust velocity gradients, e.g., $\partial u_3/\partial x_2 \simeq \Delta u_3/b'$, where Δu_3 is the spanwise change of u_3 and b' is a characteristic span distance between the finite-differencing points on the wings.

The current model, like that of Etkin, is based on von Kármán spectra, but it differs from Etkin's and most other models in two important respects. First, it is nondimensional for greater generality; and second, it utilizes spectra with finite wave-number limits, which are based on the ratios of the integral scales of turbulence to the characteristic dimensions of the Shuttle. The model, which is nonrecursive, is designed to simulate atmospheric turbulence along the flight path of the Shuttle Orbiter by generating instantaneous vertical and horizontal gusts at the vehicle center-of-gravity, and also instantaneous gust gradients. By simulating both gusts and gust gradients, the vehicle is treated as a finite-body as opposed to a point mass.[4] Such an approach is based on a first-order Taylor series expansion of the turbulent velocity field about the center-of-gravity of the vehicle.[5]

Based on the nondimensional, nonrecursive model, the dimensionless time series for both gusts and gust gradients have been generated and stored on a series of magnetic tapes that are entitled Shuttle Simulation Turbulence Tapes (SSTT). The time series are designed to represent atmospheric turbulence from ground level to an altitude of 10,000 m, and will be used by NASA in the near future for studies related to human/automatic control of the Shuttle.

II. Turbulence Generation Procedure

The nonrecursive turbulence model used to generate the SSTT is based on von Kármán spectra with finite upper limits corresponding to the dimensions of the Space Shuttle, relative to the scale of the turbulence in the atmosphere. Because the scale of turbulence increases with altitude, while the dimensions of the Space Shuttle are fixed, the finite upper limits of the von Kármán spectra increase with altitude. In order to take into account the resulting spectral changes, the atmosphere, extending from ground level to 10,000 m, was divided into four altitude bands. Sections II. A.-II. E. provide a description of the development and application of the turbulence generation procedures.

A. Selection of Atmospheric Bands

The standard deviations (σ_1, σ_2, σ_3) and the scales (L_1, L_2, L_3) of atmospheric turbulence are functions of altitude, increasing with increasing altitude, as shown in Fig. 1. Notice should be taken that the values for σ_i and L_i presented in this figure are designed for use with von Kármán spectral models and therefore differ somewhat from previously tabulated values[6] that were designed for use with Dryden spectra. Further discussion of the variation of σ_i and L_i is provided in Appendix A. Based on the variation of σ_i and L_i presented in Fig. 1, the atmosphere was divided into four altitude bands as presented in Table 1. Within each band, as also indicated in Table 1, characteristic scales of turbulence were selected for use in calculating the finite upper limit of the turbulence spectral model discussed in Sec. II. C.

B. Relative Importance of Cross-Correlations

It should be kept in mind that cross-correlations between the various components of turbulence can occur. This is particularly true in the atmospheric boundary layer, wherein horizontal turbulent momentum is transported toward the ground by turbulent eddy stresses, such that cross-correlation between u_1 and u_3, and between u_2 and u_3, can occur. Near the ground the cross-correlation coefficient R_{13} of u_1 and u_3 is given by

$$R_{13} = (u_0^*)^2/\sigma_1\sigma_3 \tag{1}$$

with $\sigma_1/u_0^* \simeq 2.5$ and $\sigma_3/u_0^* \simeq 1.4$, as given in Ref. 7. Thus, in this case, $R_{13} \simeq 0.3$. This correlation coefficient was considered sufficiently small to justify neglecting the correlation between u_1 and u_3. Similar analyses of other cross-correlations lead to the conclusion that, from a relative order-of-magnitude standpoint, all other cross-correlations can likewise be neglected.

C. Development of von Kármán Spectra with Finite Upper Limits

As developed previously,[8] the basic three-dimensional von Kármán relation to be integrated for the dimensionless gust spectra is

$$\phi_{ii}(\Omega_1,\Omega_2,\Omega_3) = \frac{55}{36a\pi^2}\,\frac{\Omega^2-\Omega_i^2}{(1+\Omega^2)^{17/6}} \tag{2}$$

The corresponding von Kármán relation for dimensionless gust gradient spectra is

$$\phi_{ii/jj}(\Omega_1,\Omega_2,\Omega_3) = \frac{55}{36\pi^2 a^3}\,\frac{\Omega_j^2(\Omega^2-\Omega_i^2)}{(1+\Omega^2)^{17/6}} \tag{3}$$

These three-dimensional spectral relations must be integrated over certain ranges of values of Ω_2 and Ω_3 to obtain one-dimensional spectral models $\Phi_{ii}(\Omega_1)$ and $\Phi_{ii/jj}(\Omega_1)$.

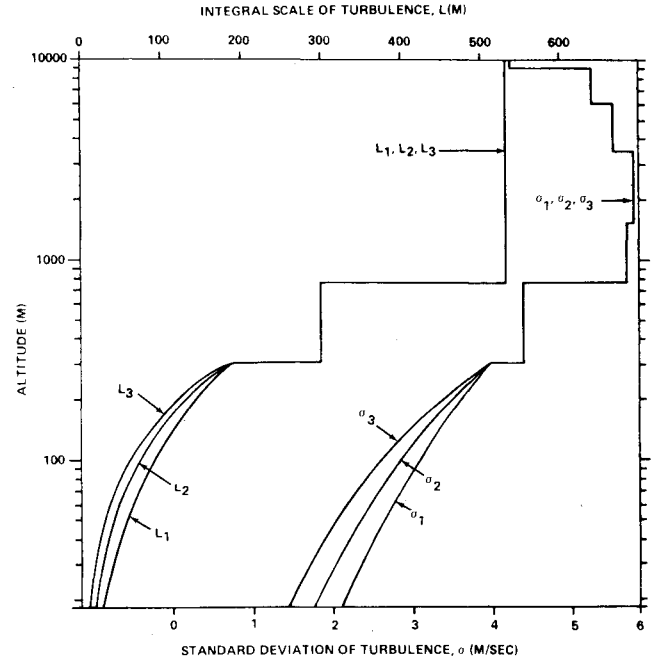

Fig. 1 Variation of von Kármán turbulence standard deviation and integral scale with altitude.

Table 1 Turbulence parameters for altitude bands

Band	Lower limit, m	Upper limit, m	Time interval (dimensionless) T	Finite limit of spectrum (dimensionless) Ω_{1max}	Ω_{2max}	Ω_{3max}	von Kármán length scale,m L_1	L_2	L_3
1	0	30	0.6018	5.22	3.38	7.22	47	30	18
2	30	100	0.2300	13.66	11.14	31.27	123	99	78
3	100	762	0.09431	33.31	33.76	120.27	300	300	300
4	762	10,000	0.05309	59.18	59.97	213.68	533	533	533

Table 2 Characteristic dimensions of the space shuttle (Ref. 10)

Characteristic length	Magnitude, m	Explanation
ℓ_1	12.06	Mean aerodynamic chord
ℓ_2	11.9	1/2 wingspan
ℓ_3	3.34	1/2 fuselage thickness

Table 3 Types of simulated turbulence

Type	Corresponding spectrum	Comments
u_1	ϕ_{11}	Longitudinal gust
u_2	ϕ_{22}	Transverse gust
u_3	ϕ_{33}	Vertical gust
$\partial u_2/\partial x_1$	$\phi_{22/11}$	Yaw
$\partial u_3/\partial x_1$	$\phi_{33/11}$	Pitch
$\partial u_3/\partial x_2$	$\phi_{33/22}$	Roll

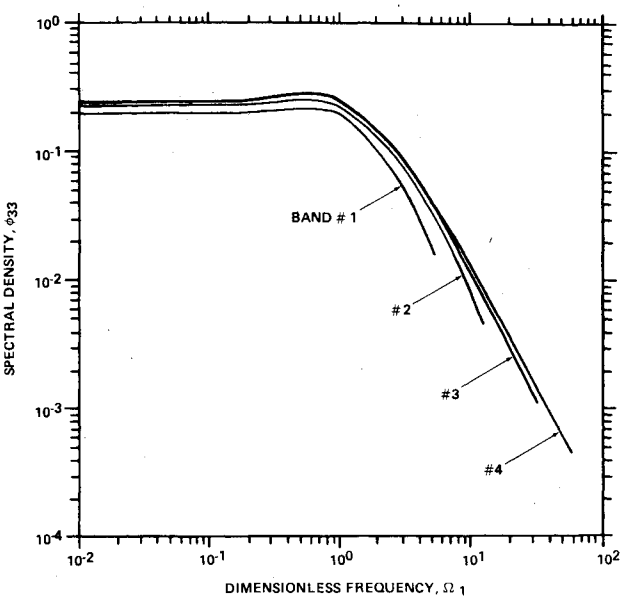

Fig. 2 Theoretical single-sided, one-dimensional spectra for u_3 gusts.

1. Upper Limits of Integration

The upper limits of integration are calculated according to the relation

$$\Omega_{imax} = aL_i/\ell_i \tag{4}$$

Equation (4) is based on the work of Etkin[4] and Filotas,[9] as described in Appendix B. Values of L_i for the four bands are given in Table 1, while the characteristic lengths, ℓ_i, are presented in Table 2. The resulting values of Ω_{imax} are included in Table 1.

2. One-Dimensional Spectra

In addition to the three gusts (u_1, u_2, and u_3) there are four gust gradients of importance ($\partial u_2/\partial x_1$, $\partial u_3/\partial x_1$, $\partial u_3/\partial x_2$, and $\partial u_1/\partial x_2$). The current Space Shuttle entry simulation models at Johnson Space Center (JSC) can accept the three gusts and the first three of the gust gradients. For this reason the turbulence simulation was limited to the six types indicated in Table 3. The mathematical model and associated numerical procedure for simulating the fourth gust gradient, $\partial u_1/\partial x_2$, are available and can be implemented if the need arises.

Based on second-order numerical integration, the six three-dimensional gust and gust gradient spectral relations corresponding to Table 3 were integrated over Ω_3 and Ω_2 (with the appropriate upper limits). Examples of the resulting one-dimensional spectra for the u_3 gusts and the $\partial u_3/\partial x_1$ gust gradients are presented in Figs. 2 and 3. Such spectra were used in establishing the impulse response functions associated with digital filter simulation processes described in Sec. II. D.

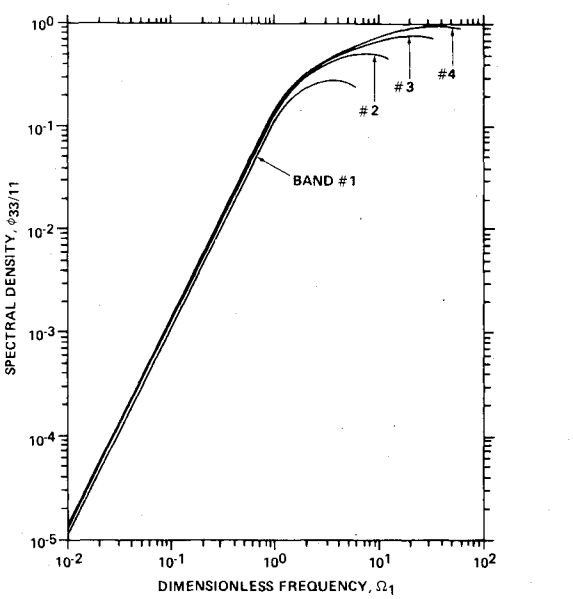

Fig. 3 Theoretical single-sided, one-dimensional spectra for $\partial u_3/\partial x_1$ gust gradients.

3. Dimensionless Energy Content

The total dimensionless energy content of each one-dimensional spectrum in each altitude band was established by integrating the corresponding spectra over the appropriate finite limit, Ω_{1max}, indicated in Table 1. The resulting energy content is presented in Table 4. As might be expected, the

Table 4 Dimensionless energy content for gusts and gust gradients

Spectrum	Altitude band 1	2	3	4
ϕ_{11}	0.5388	0.7841	0.8956	0.9298
ϕ_{22}	0.5772	0.7942	0.8952	0.9296
ϕ_{33}	0.5225	0.7646	0.8809	0.9197
$\phi_{22/11}$	1.2832	6.6484	24.768	54.125
$\phi_{33/11}$	1.1321	5.9699	22.644	49.528
$\phi_{33/22}$	0.7049	4.9954	22.893	50.057

Table 5 Index of shuttle simulation turbulence tapes (SSTT)

Tape	Time series	Comments
SSTT-1	u_1	Longitudinal gust
SSTT-2	u_2	Transverse gust
SSTT-3	u_3	Vertical gust
SSTT-4	$\partial u_2/\partial x_1$	Yaw
SSTT-5	$\partial u_3/\partial x_1$	Pitch
SSTT-6	$\partial u_3/\partial x_2$	Roll

total dimensionless energy content of each of the turbulent gust series is less than unity. The dimensionless energy** content for each gust gradient, however, is not limited in such a manner, with values ranging as high as 54.125. For both gusts and gust gradients the total energy content increases with altitude because of similar increases in the limits of integration.

D. Digital Filter Simulation

The simulated turbulence $Y(t)$ can be interpreted as the response or output of a control system [11] with a double-sided impulse response function, $h(t)$, subject to an input consisting of Gaussian white noise, $I(t)$. This response can be represented by the convolution integral

$$Y(t) = \frac{1}{2\pi}\int_{-\infty}^{\infty} h(\tau) I(t-\tau)\,\mathrm{d}\tau \tag{5}$$

Based on filter theory, the double-sided spectrum $\Phi_{DY}(\Omega)$ of the simulated turbulence satisfies the relation

$$\Phi_{DY}(\Omega_1) = H(\Omega_1) H^*(\Omega_1) \Phi_{DI}(\Omega_1) \tag{6}$$

Generally, the standard deviation of any white noise signal has a value of unity.†† Furthermore, in most practical situations the white noise is defined to occur over some interval extending from $-\Omega_{1\max}$ to $+\Omega_{1\max}$. For this case,

$$\Phi_{DI}(\Omega_1) = 1/2\Omega_{1\max} = T/2\pi \tag{7}$$

By substitution,

$$\Phi_{DY}(\Omega_1) = H(\Omega_1) H^*(\Omega_1)\,(T/2\pi) \tag{8}$$

If $H(\Omega_1)$ is limited to real values,

$$\Phi_{DY}(\Omega_1) = H^2(\Omega_1)\,(T/2\pi) \tag{9}$$

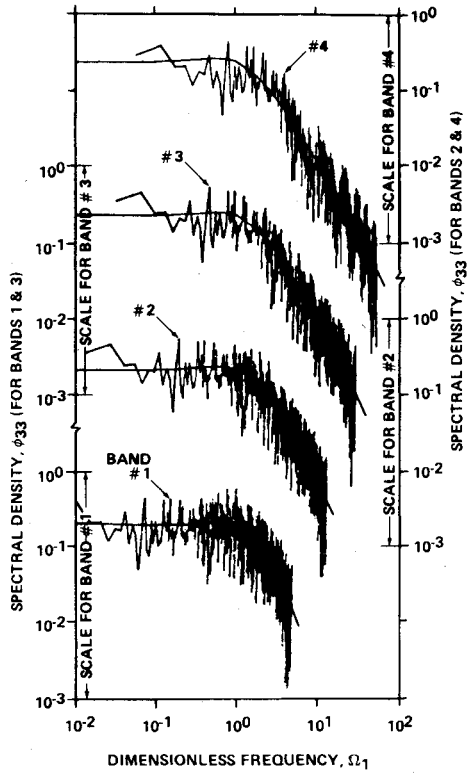

Fig. 4 Observed single-sided, one-dimensional spectra for u_3 gusts.

Rearrangement of Eq. (9) yields

$$H(\Omega_1) = \sqrt{(2\pi/T)\Phi_{DY}(\Omega_1)} \tag{10}$$

Then, based on the definition of the inverse Fourier transform, the double-sided impulse response function $h(t)$ can be expressed as

$$h(t) = \mathfrak{F}^{-1}[H(\Omega_1)] = \int_{-\infty}^{\infty} \sqrt{(2\pi/T)\Phi_{DY}(\Omega_1)}\cos(\Omega_1 t)\,\mathrm{d}\Omega_1$$

$$= 2\sqrt{(\pi/T)}\int_0^{\infty} \sqrt{\Phi_Y(\Omega_1)}\cos(\Omega_1 t)\,\mathrm{d}\Omega_1 \tag{11}$$

The single-sided spectra presented in Figs. 2 and 3 represent examples of $\Phi_Y(\Omega_1)$.

The discrete version of the convolution integral given in Eq. (5) is

$$Y(m) = \sum_{j=-N}^{+N} h(j) I(m-j)\,T \tag{12}$$

Equation (12) represents the basic, nonrecursive relation for the generation of simulated turbulence.‡‡ The impulse response functions $h(t)$ were evaluated by means of second-order numerical integration of Eq. (11), using the six spectra identified in Table 3. The values of dimensionless time increment T used for the four altitude bands are included in Table 1 and are based on the values of $\Omega_{1\max}$ shown in the same table. Thus the Nyquist generation frequencies, Ω_{NG}, for the simulated turbulence in each altitude band, correspond to the upper frequency limits for Ω_1, as computed by Eq. (4).

**Actually the term "energy" is not precise when dealing with gust gradients.

††In some derivations, [11-13] the standard deviation of the white noise signal has been set to equal $2\Omega_{1\max}$. In this case the standard deviation of the input becomes very large as $\Omega_{1\max} \to \infty$.

‡‡In Refs. 11 and 13, to correct for the "effect of digitizing," the series represented by Eq. (12) has been divided by $\sqrt{T}$. This process can be seen to be dimensionally incorrect and actually results from the use of a white noise spectrum with unit strength instead of a strength of $T/2\pi$.

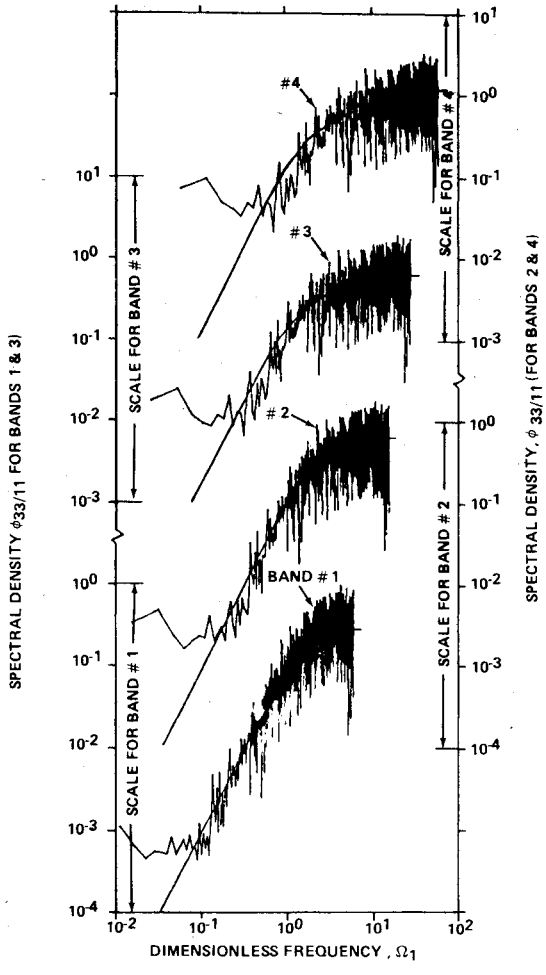

Fig. 5 Observed single-sided, one-dimensional spectra for $\partial u_3/\partial x_1$ gust gradients.

E. Effects of Digitization

The effects of digitization in turbulence simulation have been considered by a number of investigators.[11-14] As a result of these studies, two basic digitization effects have been generally identified.

The first effect results from the assumption of a white noise spectrum with unit *strength* instead of unit *power*, noted in Sec. II. D. To correct for such an "effect" the proposed procedure is to divide the series approximation of the convolution integral by $\sqrt{T}$. This effect disappears when the white noise spectrum has unit power.

The second effect involves the *tapering* of the spectrum of simulated white noise, Φ_{DI}, in the vicinity of the Nyquist generation frequency Ω_{NG}. Some investigators[12,14] have considered it necessary, because of the tapering effect, to generate the simulated turbulence time series at a rate from four to ten times the rate at which the series will be sampled. The discrete sampling process, however, results in *aliasing* of the spectrum and if the sampling frequency Ω_{NS} equals the generation frequency Ω_{NG}, spectral tapering is essentially offset by spectral aliasing.[15] In the generation of the simulated turbulence the basic assumption is made that the sampling frequency will always be approximately equal to the generation frequency, thus avoiding the second effect of digitization.

III. Simulated Turbulence Tapes

The turbulence generation procedure described in Sec. II has been used to generate six dimensionless simulated turbulence time series that are stored on magnetic tapes, as summarized in Table 5. Detailed procedures for using the tapes have been developed[16] and are available for any potential user.

Table 6 Mean value of gusts and gust gradients

Series type	Altitude band 1	2	3	4
u_1	−0.006109	−0.009637	−0.015505	−0.020793
u_2	−0.005858	−0.010306	−0.015392	−0.018100
u_3	−0.005597	−0.010238	−0.015364	−0.018100
$\partial u_2/\partial x_1$	−0.000015	−0.000269	−0.002197	−0.006183
$\partial u_3/\partial x_1$	−0.000014	−0.000270	−0.002198	−0.006188
$\partial u_3/\partial x_2$	−0.006585	−0.019388	−0.043538	−0.064540

Table 7 Standard deviation of gusts and gust gradients

Series type	Altitude band 1	2	3	4
u_1	0.724352	0.868642	0.927039	0.946672
u_2	0.756057	0.884176	0.936133	0.947373
u_3	0.719277	0.867329	0.928437	0.942133
$\partial u_2/\partial x_1$	1.139887	2.591114	4.999053	7.387333
$\partial u_3/\partial x_1$	1.670499	2.45426	4.777666	7.063241
$\partial u_3/\partial x_2$	0.836263	2.225938	4.766939	7.049476

Table 8 Ratio of square root of theoretical energy content to the observed standard deviation

Series type	Altitude band 1	2	3	4
u_1	1.0134	1.0194	1.0208	1.0186
u_2	1.0048	1.0079	1.0107	1.0177
u_3	1.0050	1.0082	1.0109	1.0179
$\partial u_2/\partial x_1$	0.9938	0.9951	0.9955	0.9959
$\partial u_3/\partial x_1$	0.9939	0.9955	0.9960	0.9964
$\partial u_3/\partial x_2$	1.0039	1.0041	1.0037	1.0036

A. Validation of Simulated Turbulence

By means of a Fast Fourier Transform,[17] spectral analyses of all simulated turbulence have been performed. Typical results are presented in dimensionless form for the u_3 gust and the $\partial u_3/\partial x_1$ gust gradient in Figs. 4 and 5. Also included in each figure is the appropriate theoretical von Kármán spectra taken from Figs. 2 and 3. The agreement between the theoretical spectra and the computed spectra is quite satisfactory. None of the computed spectra display any noticeable sign of tapering or aliasing.

Based on standard statistical analysis procedures, each of the SSTT's was analyzed to determine its mean value, standard deviation, and probability density distribution. The resulting mean values are presented in Table 6, while Table 7 contains the resulting standard deviations. As expected, all mean values were near zero.The standard deviations represent the square root of the energy content. The ratio of the square root of each theoretical energy content (from Table 4) to the corresponding standard deviation (from Table 7) is presented in Table 8. The agreement appears quite satisfactory.

Typical gust and gust gradient probability density distributions for the u_3 gust and the $\partial u_3/\partial x_1$ gust gradient are presented in Figs. 6 and 7. In each figure the corresponding

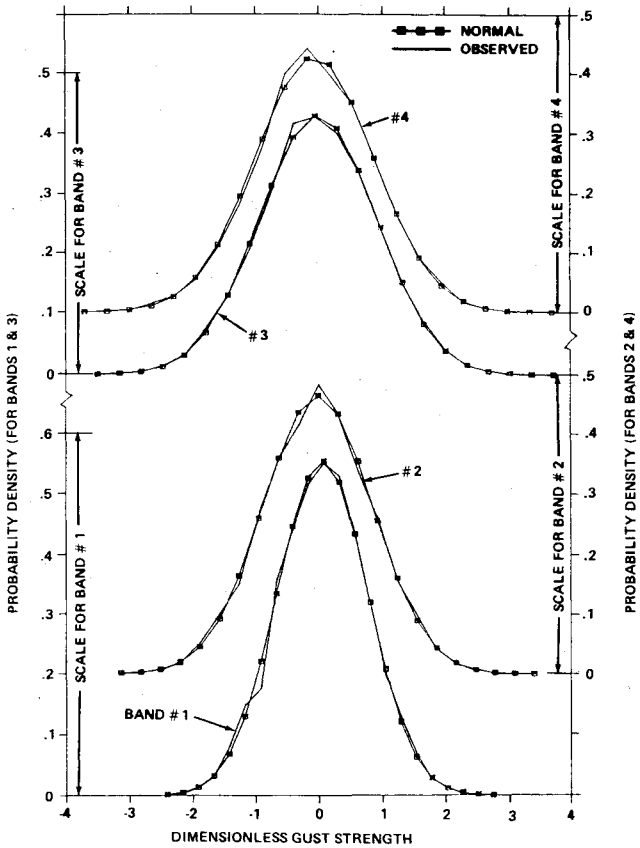

Fig. 6 Probability density distribution for u_3 gusts.

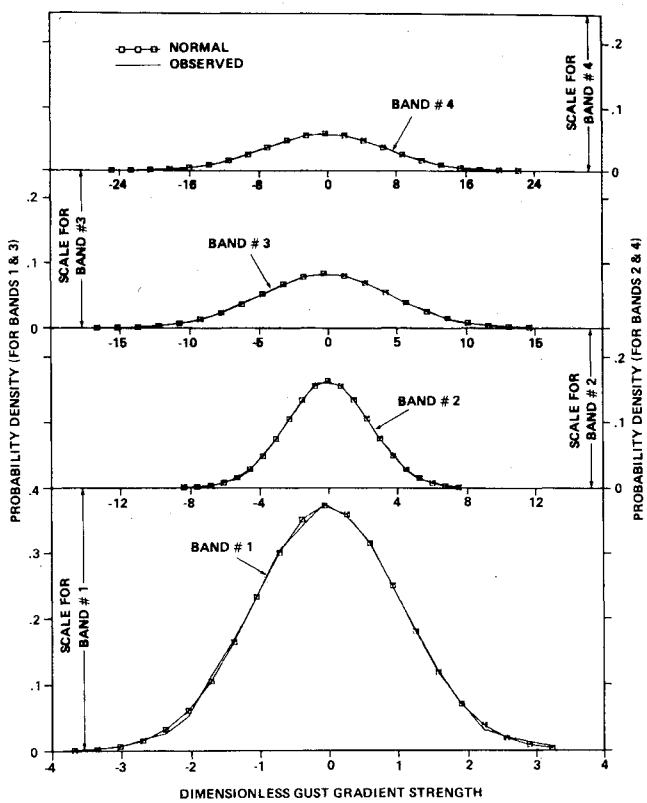

Fig. 7 Probability density distribution for $\partial u_3/\partial x_1$ gust gradients.

normal distribution is also presented. The results indicate that both the gust and gust gradient time series are very close to normal distributions.

B. Conversion to Dimensional Values

The dimensionless time series on each tape must be converted to dimensional form before actual use in a simulation exercise. The conversion process generally involves multiplication and/or division by the appropriate turbulence parameters. For dimensionless gusts u_i, the corresponding standard deviation σ_i should be used. Thus,

$$u_i' = \sigma_i u_i \tag{13}$$

For dimensionless gust gradient $\partial u_i/\partial x_j$, the parameters σ_i and L_i are used. Thus

$$\frac{\partial u_i'}{\partial x_j'} = \frac{\sigma_i}{L_i}\frac{\partial u_i}{\partial x_j} \tag{14}$$

In the case of dimensionless time, for converting to dimensional form, the dimensionless time step represents the basic unit to be converted. The conversion involves the vehicle velocity V and the appropriate turbulence scale L_i. Thus

$$\Delta t_i' = aL_i T/V \tag{15}$$

It is important to note that because both L_i and V vary with altitude, the resulting dimensional time step $\Delta t_i'$ is not a constant. To obtain dimensional time t_i', a summation process is involved as follows:

$$t_{iN}' = \sum_{n=1}^{N} \Delta t_{in}'$$

$$= aT \sum_{n=1}^{N} L_{in}/V_n \tag{16}$$

Table 9 Typical variation of shuttle velocity with altitude (Ref. 14)

Altitude, m	V, m s^{-1}
100	152
300	156
500	158
2,000	170
4,000	188
6,000	200
8,000	240
10,000	300

The variation of the turbulence standard deviation σ_i with altitude was presented in Fig. 1. The same figure contains the turbulence scale L_i as a function of altitude. The vehicle speed V is a function of altitude, but also may vary from one trajectory to another. Table 9 provides *representative* values of V as a function of altitude.

IV. Concluding Remarks

By means of a nonrecursive discrete generation process, based on a von Kármán spectral model with finite upper limits, dimensionless simulated turbulence time series have been developed and stored on six magnetic tapes. Longitudinal, transverse, and vertical gusts are simulated as well as the gust gradients associated with yaw, pitch, and roll. For each gust or gust gradient four separate time series (corresponding to four altitude bands extending from ground level to 10,000 m) have been stored on each tape.

The results of spectral analyses of each tape reveal that the simulated turbulence possesses the appropriate von Kármán spectral characteristics. Statistical analyses of the tapes indicate that both the simulated gust and gust gradients are normally distributed with near-zero means. Furthermore, the standard deviation of each series is consistent with the theoretical energy content.

The Shuttle Simulation Turbulence Tapes (SSTT) are now ready for actual use for simulating turbulence at altitudes below 10,000 m and appropriate steps are currently being taken to incorporate the tapes into existing simulation systems. In addition, by means of the same model, simulated turbulence is presently being generated for altitudes between 10,000 and 100,000 m. Although originally developed for the Space Shuttle, the SSTT have potential application to other aeronautical and aerospace systems.

Appendix A: Derivation of von Kármán Values of Standard Deviation and Turbulence Scale from Dryden Values

The variations of σ_i and L_i with altitude for von Kármán spectral models, as presented in Fig. 1, are based on similar variations for Dryden spectral models as contained in JSC 07700.[6] For the latter case the profiles of length scales L_i below the 304.8-m level were obtained by using currently available information about L as a function of altitude z near the ground ($z \lesssim 30$ m). This information is in the form of one-dimensional autospectra of u_i ($i=1,2,3$) for radian wave-number k_1 (in the x_1 direction) derived primarily from time histories of wind measured with sensors located on towers.

The measured spectra are in the frequency domain and were converted to spectra in the wave-number domain by applying Taylor's hypothesis. According to Taylor's hypothesis, turbulent eddies are frozen into the mean flow and the radian frequency ω of an eddy relative to an observer on the tower is related to the radian wave-number k_1 in the direction of the mean wind (obtained, for example, by applying a 10 min average), or rather in the direction along which the atmosphere is being probed, so that

$$k_1 = \bar{u}\omega \tag{A1}$$

where $\bar{u}$ is the mean wind. The vertical variation of L near the ground appropriate for a Dryden spectral model were then obtained by matching Dryden representation to the empirical representations.[18] Values of L (appropriate for a Dryden model) were then derived for the 18.3-m level, which is the level to which all ground winds are referenced at the Kennedy Space Center (KSC), for statistical specification of design criteria for the Space Shuttle in Ref. 6.

The distribution of L at and above the 304.8-m level was obtained from Ref. 7. These data were derived from aircraft response data sets.[19] Power law profiles were used to interpolate the values of L between the 18.3- and 304.8-m levels. Such profiles were based on the assumption that the turbulence at the 304.8-m level and above is fully isotropic and only locally isotropic at the 18.3-m level for asymptotically large values of k_i; i.e., L is a function of height z (above the natural grade), and is given by

$$L_i(z) = L_i(18.3)\,(z/18.3)^{q_i} \tag{A2}$$

where q_i is a nondimensional parameter. It was further assumed that for engineering purposes the resulting profiles of integral scale of turbulence could be used for all wind conditions.

The derivation of the profiles of σ was somewhat more involved. First, it should be recognized that distributions of σ in JSC 07700 are envelopes of σ based on the accepted risk of exceeding the Shuttle Orbiter landing wind speed at the 18.3-m level for the worst hour of the worst month of the year and on the accepted value of risk of exceeding the design value of σ at the 304.8-m level and above for a given period of exposure t_e'. Furthermore, the design envelope approach is used for establishing design values of σ and above the 304.8-m level; i.e., the total number of flying hours is assumed to occur at each altitude.

The distribution function of peak wind speed at the 18.3-m level for the worst hour of the worst month (envelope distribution of the monthly peak wind distributions for each hour) was used to establish the design peak wind at the 18.3-m level at the 1% risk level. The peak winds were then used to establish design values of σ at the 18.3-m level by a series of steps which involved 1) converting the design landing peak wind speed to mean wind by applying a gust factor; 2) calculating surface friction velocity u_0^* with the logarithmic mean wind profile and an estimate of ground roughness at Cape Kennedy and Vandenberg AFB; and 3) then calculating the values of σ from u_0^*.

The design value of σ at the 304.8-m level was obtained from empirically derived gust exceedance curves.[7] These curves consist of the expected number of exceedances $M(\xi)$ of gust velocity per unit time, as a function of threshold value ξ. In the design envelope approach the total expected number of hours, t_e', for which the Space Orbiter is anticipated to be exposed to the atmosphere during entry over its expected lifetime, is used to derive an exceedance rate M at each altitude above the 304.8-m level. Given the risk of exceedance of the design gust is 63%, and based on a Poisson failure model, the exceedance rate relation is

$$M = 1/t_e' \tag{A3}$$

Thus specification of t_e' yields M, which can then be used to derive a vertical profile envelope of ξ at and above the 304.8-m level. Finally, it is assumed that the design gust velocity at each altitude above the 304.8-m level occurred in a patch of turbulence with standard deviation σ such that $\xi = 3.5\sigma$, to establish the profile envelope of σ at and above the 304.8-m level.

The distributions of σ between the 18.3- and 304.8-m levels were then obtained by fitting a power law of the form

$$\sigma_i(z) = \sigma_i(18.3)\,(z/18.3)^{p_i} \tag{A4}$$

where p_i is a nondimensional constant. Minimum values of σ ($\sigma_1 = \sigma_2 = 2.44$ m s^{-1}, $\sigma_3 = 2.13$ m s^{-1}) and L ($L_1 = L_2 = L_3 = 10$ m) are also used for assessment of landing performance, handling qualification evaluation, and performing in-flight and ground simulation and in-flight control analysis of flights subsequent to the first Shuttle mission.[6]

The preceding discussion has dealt with the procedures followed in establishing the variations of σ_i and L_i with altitude for Dryden spectral models, as presented in JSC 07700.[6] For more details dealing with such variations for Dryden spectral models the reader is referred to Refs. 7 and 20.

In developing values of σ_i and L_i for von Kármán spectra, the basic requirement is to satisfy the local isotropy relation

$$\sigma_1^2/L_1^{2/3} = \sigma_2^2/L_2^{2/3} = \sigma_3^2/L_3^{2/3} \tag{A5}$$

From 304.8 to 10,000 m, Dryden values of σ_i and L_i satisfy Eq. (A5) and thus can be used with the von Kármán model. Below 304.8 m the procedure[19] for converting to von Kármán values involves utilizing Dryden reference values of σ_3, L_1, L_2, and L_3 at 18.3 m in conjunction with Eq. (A5) to obtain reference values of σ_1 and σ_2 at the same altitude. In addition, at 304.8 m the von Kármán values for σ_i and L_i are assumed to equal their Dryden counterparts. With values of σ_i and L_i established at 18.3 and 304.8 m, both parameters are assumed to vary with altitude in accordance with Eqs. (A2) and (A4) (except that the von Kármán values of the exponents p_1 and p_2 will differ from the corresponding Dryden values).

By means of the conversion process described, the Dryden values of σ_i and L_i from JSC 07700 (Ref. 6) were converted into the von Kármán values presented in Fig. 1.

Appendix B: Finite Limits for Spectra

According to Etkin,[4] for unsteady, oscillatory aerodynamic analysis, with the first-order power series approach

for a finite aircraft, the limit of k_1 is given by

$$k_1 \ell_1 / 2 < 0.5 \tag{B1a}$$

or

$$k_1 < 1/\ell_1 \tag{B1b}$$

where ℓ_1 is the mean aerodynamic chord.

The limit for k_2 results from the approximate solution for rolling moment of Filotas,[9] which, as shown by Etkin,[4] for the linear power series approximation, should satisfy the inequality

$$k_2 \ell_2 < 1 \tag{B2a}$$

or

$$k_2 < 1/\ell_2 \tag{B2b}$$

where ℓ_2 is one-half of the wing span.

No limit for k_3 has been rigorously developed in the past, but analogous to the derivation leading to the limit for k_2, for a first-order power series approximation,

$$k_3 \ell_3 < 1 \tag{B3a}$$

or

$$k_3 < 1/\ell_3 \tag{B3b}$$

where ℓ_3 is the characteristic vertical dimension of aircraft.

The three preceding inequalities can be expressed in dimensionless form as

$$\Omega_i < aL_i/\ell_i \tag{B4}$$

The maximum value of Ω_i can thus be set as

$$\Omega_{i\max} = aL_i/\ell_i \tag{B5}$$

References

[1] Etkin, B., "The Turbulent Wind and Its Effect on Flight," AIAA Paper 80-1836, Aug. 1980.

[2] Skelton, G. B., "Investigation of the Effects of Gusts in V/STOL Craft in Transition and Hover," AFFDL-TR-68-85, 1968.

[3] Holley, W. E. and Bryson, A. E. Jr., "Wind Modelling and Lateral Control for Automatic Landing," *Journal of Spacecraft and Rockets,* Vol. 14, Feb. 1977, pp. 65-72.

[4] Etkin, B., *Dynamics of Atmospheric Flight,* John Wiley and Sons, Inc., New York, 1972.

[5] Etkin, B., "Theory of the Flight of Airplanes in Isotropic Turbulence—Review and Extension," Report 372, North Atlantic Treaty Organization, April 1961.

[6] Space Shuttle Program: "Natural Environment Design Requirements. Appendix 10.10, Space Shuttle Flight and Ground Specification, Level II Program Definition and Requirements," JSC 07700, Vol. X, Revision C., NASA-Lyndon B. Johnson Space Center, Houston, Texas, Aug. 18, 1975.

[7] Kaufman, J. W., ed., "Terrestrial Environment (Climatic) Criteria Guidelines for Use in Aerospace Vehicle Development, 1977 Revision," NASA TM 78118, 1977.

[8] Tatom, F. B. and Smith, S. R., "Atmospheric Turbulence Simulation for Shuttle Orbiter," EAI-TR-79-004, Engineering Analysis, Inc., Huntsville, Ala., Aug. 31, 1979.

[9] Filotas, L. T., "Approximate Transfer Functions for Large Aspect Ratio Wings in Turbulent Flow," *Journal of Aircraft,* Vol. 8, June 1971, pp. 395-400.

[10] Rockwell International Corporation, "Aerodynamic Design Substantiation Report," SD74-SH-0205, 1974.

[11] Fichtl, G. H., Perlmutter, M., and Frost, W., *Handbook of Turbulence,* Plenum Publishing Corp., New York, 1977, Vol. 1, Chap. 14.

[12] Newman, F. and Foster, J. D., "Investigation of a Digital Automatic Aircraft Landing System in Turbulence," NASA TN D-66066, Oct. 1970.

[13] Perlmutter, M., "Stochastic Simulation of Ocean Waves for SRB Simulation," NASA TR-230-1446, May 1975.

[14] Fichtl, G. H., "A Technique for Simulating Turbulence for Aerospace Vehicle Flight Simulation Series," NASA TM 78141, Nov. 1977.

[15] Tatom, F. B. and Smith, S. R., "Space Shuttle Simulation Model," EAI-TR-80-003A, Summary Report, Engineering Analysis, Inc., Huntsville, Ala., Nov. 17, 1980.

[16] Tatom, F. B. and Smith, S. R., "Shuttle Simulation Turbulence Tapes (SSTT) Users Guide," EAI-TR-80-002A, Engineering Analysis, Inc., Huntsville, Ala., Oct. 27, 1980.

[17] Maynard, H. W., "An Evaluation of Ten Fast Fourier Transform (FFT) Programs," Research and Development Technical Report ECOM-5476, U. S. Army Electronics Command, Fort Monmouth, N.J., March 1973.

[18] Luers, J. K., "A Model of Wind Shear and Turbulence in the Surface Boundary Layer," NASA CR-2288, July 1973.

[19] Chalk, C. R. et al., "Background Information and User Guide for MIL-F-8785B(ASG), Military Specification—Flying Qualities of Piloted Airplanes," AFFDL-TR-69-72, Aug. 1969.

[20] Fichtl, G. H., "Problems in the Simulation of Atmospheric Boundary Layer Flows," AGARD-CP-140(1973)2-1, AGARD Flight Mechanics Panel Symposium on Flight in Turbulence, Great Britain, May 1973.